Manufacturing and Properties of Biobased Thermoplastic Composites From Poly(lactid acid) and Hazelnut Shell Wastes

J.F. Balart, D. García-Sanoguera, R. Balart, T. Boronat, L. Sánchez-Nacher
Instituto de Tecnología de Materiales (ITM), Universitat Politècnica de Valencia (UPV), Plaza Ferrandiz-Carbonell, s/n, 03801 Alcoy, Alicante, Spain

Poly(lactic acid), PLA-based green composites were obtained with hazelnut shell flour (HSF) derived from the food industry thus leading to fully biodegradable materials with attracting properties. The hazelnut shell flour content varied in the 10–40 wt% range. An increase in the degree of crystallinity with increasing HSF was detected, mainly due to the nucleating effect of lignocellulosic particles. The thermodimensional stability was noticeably improved with increasing HSF amount as evidenced by a remarkable decrease in the coefficient of thermal–linear expansion. Increasing HSF leads to stiffer materials as HSF particles act as interlock points that restrict polymer chain motion. Addition of hazelnut shell flour as filler in PLA-based green composites leads to fully biodegradable composites with balanced mechanical and thermal properties. Furthermore, it gives a solution to upgrade wastes from the hazelnut industry and contributes to lower the cost of PLA-based materials. POLYM. COMPOS., 39:848–857, 2018. © 2016 Society of Plastics Engineers

INTRODUCTION

Recent and increasing concerns about environment protection, sustainability petroleum depletion and use of renewable resources have promoted the need of new ecoefficient materials. These environmentally friendly materials contribute to sustainable development by minimizing wastes at the end of the life cycle with potential recycling, upgrading, and/or biodegradation thus leading to low environmental impact.

In this field, research has paid special interest on new polymeric materials from renewable resources and/or potentially biodegradable. Natural origin means no petroleum dependency, which is positive to avoid petroleum depletion. Biodegradation means environment protection as no harmful/durable wastes are generated; on the other hand, biodegradation allows readily decomposition of polymers in comparison to petroleum-based polymers (i.e., poly(ethylene) and poly(propylene) takes 100–150 years to fully degrade). Al the research on biobased and/or biodegradable polymers has led to a wide variety of materials, most of them currently commercially available. Biopolymers from natural resources are characterized by physicochemical properties similar to petroleum-based polymers. Biopolymers can be divided into three main families. One group includes all polymers coming from biomass: polysaccharides such as starch, cellulose, chitosan, etc. and proteins such as casein, keratin, collagen, gluten, etc. Some polymers can be obtained by chemical synthesis using biological monomers from renewable resources, such as poly(-lactic acid)—PLA or poly(glycolic acid)—PGA. Finally, it is possible to find biopolymers obtained by controlled bacterial fermentation as polyhydroxyalkanoates (PHAs), such as poly(hydroxy butyrate)—PHB or poly(hydroxy butyrate co valerate—PHBV [1, 2].

One of the most used biopolymers at industrial level is poly(lactic acid)–PLA with an annual consumption of 140,000 tonnes per year. PLA can be obtained from monomers that are readily available from sugar rich compounds, cellulose and starches such as potato, corn, wheat, sugarcane, etc. [2–4] PLA is a thermoplastic polymer characterized by high fragility and similar mechanical properties to poly(styrene)—PS. Production of PLA begins with the starch obtained from corn and then some microorganisms convert this into a shorter molecule of lactic acid that is the base monomer for PLA production. Conventional PLA is characterized by a crystallinity degree (X_c) of about 37%, a glass transition temperature (T_g) between 60°C and 65°C, a melt temperature (T_m) in the 173–175°C range and an elastic modulus between 2.7 and 16 GPa [5].

PLA can be processed in a similar way to commodity plastics. The most common uses of PLA include disposable and compostable glasses for cold drinks, bags, and

Correspondence to: J. F. Balart; e-mail: jfbalart@dimm.upv.es
Contract grant sponsor: Ministerio de Economía y Competitividad—MINECO; contract grant number: MAT2014-59242-C2-1-R; contract grant sponsor: Conselleria d'Educació, Cultura i Esport; contract grant number: GV/2014/008.
DOI 10.1002/pc.24007
Published online in Wiley Online Library (wileyonlinelibrary.com).

packages for food, teabags, disposable plates, and cutlery, etc. PLA (medical grade) is also used for biomedical applications such as resorbable stitches, stents, drug delivery carriers, etc. [6–15]

As PLA offers similar properties to some commodities, one attracting application is its use as matrix in fully biodegradable wood plastic composites (WPCs) which are composed of a polymer matrix and a lignocellulosic filler thus leading to materials with similar appearance to wood. In the last decades an increasing interest on natural fiber reinforced plastics (NFRPs) with lignocellulosic fibers, such as hemp, jute, kenaf, flax, henequen, *Posidonia oceanica* seaweed, etc. has been detected [2, 13–21]. Nevertheless, conventional WPCs with petroleum-based polymers, such as poly(ethylene)—PE, poly(propylene)—PP, poly(vinyl chloride)—PVC, and others have a negative impact during and at the end of the life cycle [22, 23]. The use of WPCs is increasing in a remarkable way as they offer easy processing by conventional processing techniques (injection, extrusion, etc.); they also offer shape versatility, cost effective, and lightweight materials, balanced resistance to external agents, good resistance to salt and sand, attractive surface finishing, etc. WPCs represent a remarkable high market share in the building sector with uses in decking, solar diffuser, facades, interior floor, profiles, pergola, fencing, handrails, etc. [24]. In Europe, WPCs are mainly used in the automotive sector in interior parts [2, 25–28].

The new generation of WPCs are called "green composites" or "biobased thermoplastic composites" and are characterized by the use of a biopolymer matrix together with a lignocellulosic filler from industrial wastes; these components allow obtaining fully biodegradable WPCs with high environmental efficiency [25, 29–32]. Although the typical lignocellulosic filler in WPCs is sawdust from the wood industry, the use of lignocellulosic wastes obtained from agroforest and food industry is increasing continuously. In the last decades, a wide variety of lignocellulosic materials, such as husk rice, almond husk, spent coffee grounds, cotton gin waste, pine needle, stalks of cereal crops, corncobs, peanut shells, etc. have been proposed for green composites [33, 34].

The annual crop of hazelnut is about 800,000 tonnes. It is worth to note that the hazelnut shell represents between 50% and 60% of the total weight thus leading to an important amount of wastes around the world. These lignocellulosic wastes can be used as biomass fuel for different industries. Despite this, these wastes can be powdered to give hazelnut shell flour with similar appearance to wood. In addition, hazelnut shell is characterized by a relatively low density as other lignocellulosic filers. Copur et al. determined the composition of the hazelnut shell resulting in 55.1% holocellulose, 34.5% α-cellulose, 35.1% lignin and 8.2% ashes. It is important to remark the high lignin content that leads to hard shells [23, 35–37].

The aim of this research work is the development of biobased thermoplastic composites from poly(lactic acid)–PLA and hazelnut shell wastes to assess their potential as WPCs with potential uses in technical applications. The effect of the hazelnut content is evaluated in terms of the mechanical, thermal and thermomechanical properties of PLA/HSF composites.

EXPERIMENTAL

Materials

A poly(lactic acid)–PLA commercial grade Ingeo 6201D supplied by NatureWorks LLC (Minnesota, USA) was used as matrix for composites. This PLA possesses a density of 1.18 g cm^{-3} and a melt flow index of 15–30 g/10 min at 210°C. Hazelnut shell (*Corylus avellana* variety) obtained as a byproduct of the food industry was used as lignocellulosic filler for composites.

Composite Manufacturing

Prior to further processing, hazelnut shell was grinded in an ultracentrifugal mill (Retsch GmbH, Hann, Germany) at a rotating speed of 10,000 rpm. After this, the powdered hazelnut shell flour was dried at 60°C for 24 h. Particle size and distribution is shown in Fig. 1 with predominant particle size lower than 63 μm.

PLA was subjected to the same drying process (60°C for 24 h) to remove residual moisture. PLA/HSF composites were manufactured as follows: initially, exact amounts of PLA and HSF were weighed and mechanically mixed in a zipper bag to homogenize. The HSF content was varied in the 10–40 wt%. After the initial homogenization, mixtures were compounded in a twin screw corotating extruder from DUPRA S.L. (Alicante, Spain) with a temperature profile of 176°C (hopper), 180°C, 185°C, and 192°C (day) at a constant rotating speed of 40 rpm. The obtained compounds were pelletized for further processing by injection molding in a Meteor 270/75 from Mateu and Solé (Barcelona, Spain) to obtain standard samples for testing.

PLA/HSF Composite Characterization

Thermal characterization of PLA/HSF composites was carried out by differential scanning calorimetry (DSC) in a Mettler–Toledo DSC mod. 821 (Schwerzenbach, Switzerland). Dynamic DSC analysis was carried out in three consecutive temperature steps. The first step (heating from 30°C to 200°C at 10°C min^{-1}) was applied to remove the previous thermal history due to prior processing. After this, a controlled cooling cycle (from 200°C to −50°C at −10°C min^{-1}) was applied to slowly cool PLA and, finally, the last step was a heating program from −50°C to 350°C at 10°C min^{-1} which is the base cycle for determining all thermal parameters. All three steps

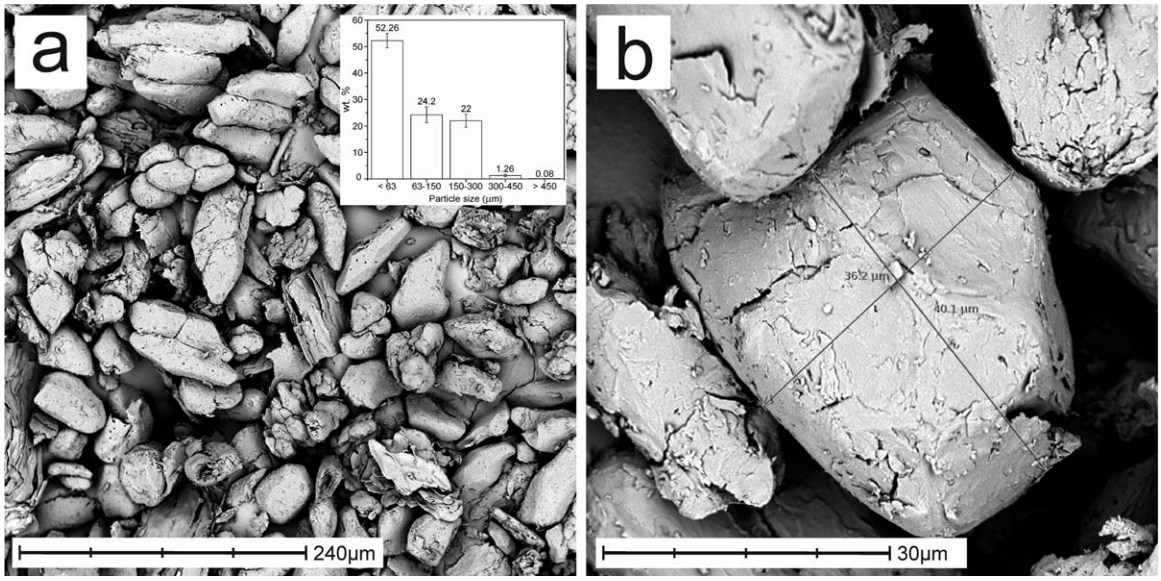

FIG. 1. SEM image showing the hazelnut shell flour surface morphology, (a) rounded shapes with similar size at 500× and (b) simple size measurement at 4000×.

were carried out under nitrogen atmosphere (66 mL min^{-1}).

The crystallinity degree of PLA (X_{cPLA}) was calculated from DSC thermograms by using the following equation:

$$X_{cPLA}(\%) = \left[\frac{|\Delta H_m| - |\Delta H_{cc}|}{|\Delta H_{100\%}| \cdot w_{PLA}}\right] \times 100 \quad (1)$$

where ΔH_m is the melt enthalpy, ΔH_{cc} is the cold crystallization enthalpy, $\Delta H_{100\%}$ is the theoretical melt enthalpy for 100% crystalline PLA (−93.7 J g^{-1}), and w_{PLA} is the weight fraction of PLA in PLA/HSF composites [7, 8, 11, 38, 39].

Thermal degradation of PLA/HSF composites was followed by thermogravymetric analysis (TGA) in a horizontal thermobalance Mettler-Toledo TGA/SDTA 851 (Schwerzenbach, Switzerland) with a temperature program from 30°C to 700°C at 20°C min^{-1} in nitrogen atmosphere (66 mL min^{-1}).

Thermomechanical properties of PLA/HSF composites were evaluated by measuring the Vicat softening temperature (VST) and heat deflection temperature (HDT) in a VICAT/HDT station mod. VHDT 20 from Metrotec S.A. (San Sebastián, Spain). VST tests were carried out as indicated in ISO306 with a load of 5 kg and a heating rate of 50°C h^{-1}. With regard to HDT test, the ISO 75 (ASTM D 648) was followed with a load of 296 g and a heating rate of 120°C h^{-1}. In addition, the coefficient of linear thermal expansion (CLTE) of PLA/HSF composites was determined in a TMA analyzer from TA Instruments mod. Q400 (Delaware, USA). The heating program was set from −100°C to 80°C at a heating rate of 3°C min^{-1} and a constant force of 0.02 N.

Mechanical characterization of PLA/HSF composites was carried out by flexural, impact and hardness tests. The flexural test was done as described in the ISO 178 standard with rectangular samples sizing 10 × 80 × 4 mm^3 in a universal machine ELIB 30 from S.A.E. Ibertest (Madrid, Spain). The load cell was 5 kN and the crosshead speed was 5 mm min^{-1}. The flexural deformation (ε_f), strength (σ_f), and modulus (E_f) were calculated following these equations:

$$\varepsilon_f = \frac{6 \cdot s \cdot h}{L^2} \quad (2)$$

$$\sigma_f = \frac{3 \cdot F \cdot L}{2 \cdot b \cdot h^2} \quad (3)$$

$$E_f = \frac{\sigma_{f2} - \sigma_{f1}}{\varepsilon_{f2} - \varepsilon_{f1}} \quad (4)$$

where s is the sample deflection (mm), h is the sample thickness (mm), L is the distance between supports (mm), F is the applied force (N), b is the sample width (mm). The flexural modulus is calculated as the ratio between the change in flexural stress ($\sigma_{f2} - \sigma_{f1}$) and the difference between two flexural deformations of ε_{f2} (0.0025)–ε_{f1} (0.0005).

The impact absorbed energy was determined following ISO 179 standard in a Charpy pendulum (1 J) on unnotched samples with dimensions 10 × 80 × 4 mm^3. With regard to hardness, Shore D values of PLA/HSF composites were measured using a shore D durometer mod. 673-D from J. Bot S.A. (Barcelona, Spain). At least five different samples were tested for each mechanical test and average values of the corresponding parameters were calculated.

Morphology of fractured surfaces from impact tests was evaluated with scanning electron microscopy (SEM) in a PHENOM microscope from FEI Company (Eindhoven, The Netherlands). The acceleration voltage was 5 kV and prior to surface observation, samples were subjected to a sputtering process with an aurum–palladium

 DOI 10.1002/pc

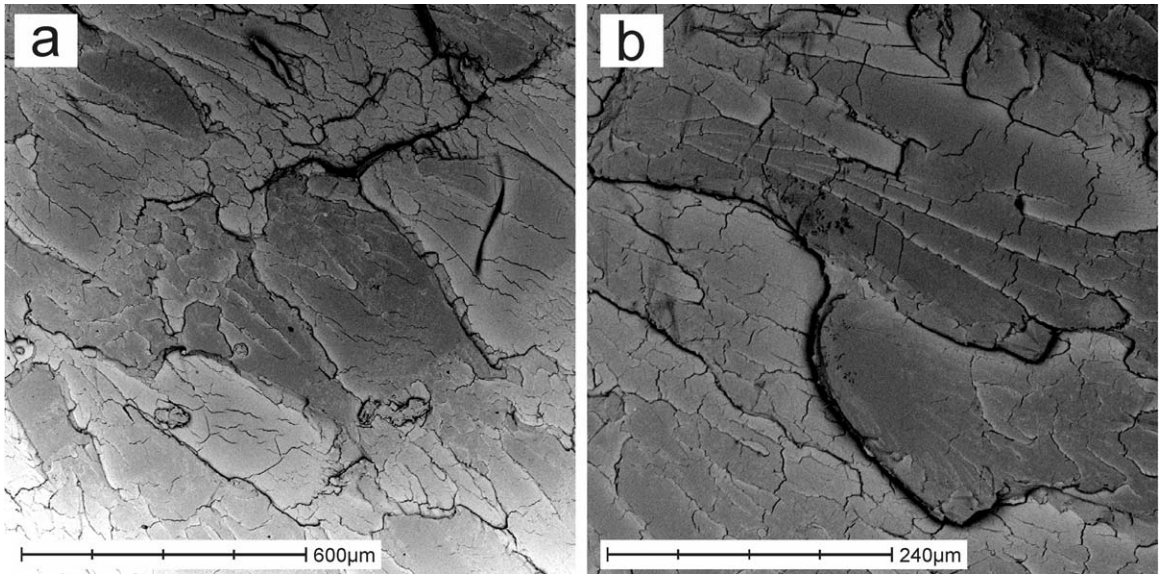

FIG. 2. SEM image showing the morphology of the impact-fractured surface of unfilled PLA at different magnifications, (a) 200× and (b) 500×.

alloy in a sputter-coated mod. EMITECH mod. SC7620 from Quorum Technologies (Sussex, UK).

RESULTS AND DISCUSSION

Surface Morphology of PLA/HSF Composites

Surface morphology of fractured samples from impact tests was evaluated by scanning electron microscopy to qualitatively assess particle–polymer interactions. Figure 2 shows the typical surface morphology of unfilled PLA. It is possible to observe some irregularities with different linear microcrack fronts representative for fragile fracture. No evidences of plastic deformation can be detected so that, typical fracture is characterized by highly smooth surfaces.

Figure 3 shows the surface morphology of fractured PLA/HSF composites with different HSF content (20 and 30 wt% as representative images). It is possible to observe quite well dispersed hazelnut shell particles surrounded by PLA matrix thus indicating that compounding with twin-screw corotating extruder followed by injection moulding is appropriate to achieved good particle dispersion. In addition, previous drying of both components allows obtaining composite materials without typical porosity caused by moisture. Fracture surface is quite regular and homogeneous with small roughness due to the impact but no evidences of plastic deformation can be observed. It is clearly detectable the lack of strong interactions between the lignocellulosic hazelnut shell powder and the surrounding PLA matrix, which gives evidences of the poor particle–polymer interface adhesion. It is possible that some hydroxyl groups in cellulose could react with PLA end chains but this has not a relevant influence on microstructure. This phenomenon leads to lack of particle–polymer continuity, which is responsible for stress concentration phenomena and poor load transfer from the particle to the matrix. There is a high surface area covered by HSF particles. Due to the lack of interaction, the sum of all the gaps between particles and surrounding matrix increases with the HSF content thus leading to early fracture [6–9, 13, 14, 17, 23, 26, 27]. This could be minimized by surface treatment of HSF or by adding coupling agents and/or compatibilizers as reported in bibliography [40, 41].

Thermal Properties of PLA/HSF Composites

Figure 4 shows a comparative plot of the DSC thermograms corresponding to unfilled PLA and PLA composites with different HSF content.

As it can be observed, all samples show a step in the baseline at about 60–70°C which corresponds to PLA glass transition temperature (T_g). By taking the T_g at the inflection point, its value is located at around 66.5°C. Addition of HSF particles do not lead to a remarkable change in T_g as observed by DSC analysis; this can be representative for lack of interaction (or very low) between the hazelnut shell powder and the surrounding PLA matrix [4]. The first exothermic peak in the DSC curves is related to the cold crystallization process due to polymer chain rearrangement. The cold crystallization temperature (T_{cc}) for unfilled PLA is located at about 111.5°C. The addition of HSF filler leads to a slight decrease in the T_{cc} values up to 104°C. This decrease in the cold crystallization temperature is due to presence of lignocellulosic particles from hazelnut shell that enables early crystallization as they provide a nucleating effect. On the other hand, the total amount of HSF does not affect the T_{cc} value in a noticeable way. The second peak (endothermic) corresponds to PLA melting. Unfilled PLA

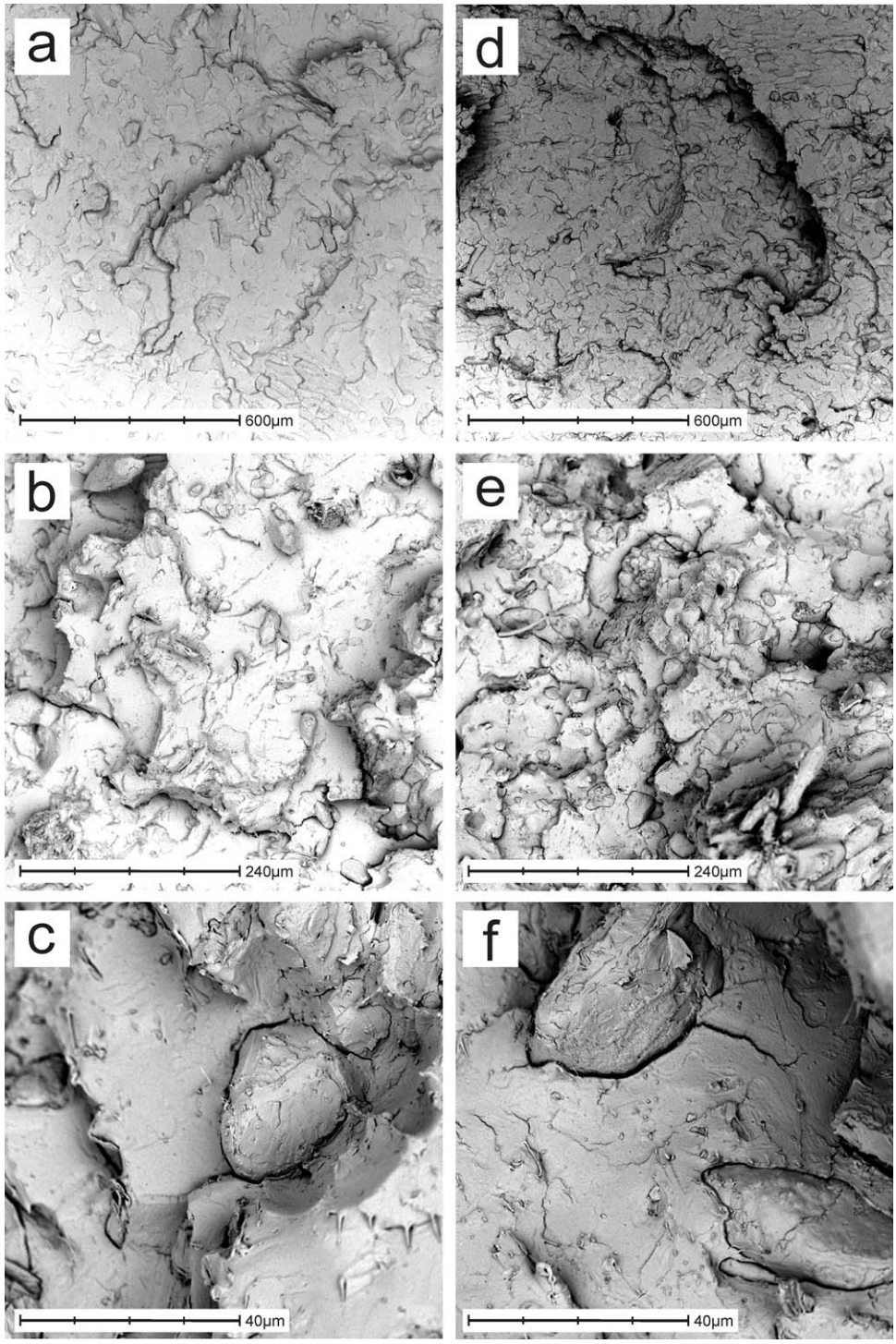

FIG. 3. SEM images showing the IMPACT-fractured surfaces of PLA/HSF composites with different HSF content and different magnifications, (a) 20 wt% HSF, 200×, (b) 20 wt% HSF, 500×, (c) 20 wt% HSF, 3000×, (d) 30 wt% HSF, 200×, (e) 30 wt% HSF, 500×, (f) 30 wt% HSF, 3000×.

melts at 170.8°C and no significant changes are obtained for PLA/HSF composites with different HSF content (i.e., the melt temperature for a PLA/HSF composite with 40 wt% HSF is 169°C).

Table 1 summarizes the main thermal parameters obtained from DSC analysis. The normalized enthalpies for the cold crystallization and melting (ΔH_{cc} and ΔH_m, respectively) are obtained by dividing the corresponding enthalpy (peak integral) values between the total weight of the samples; nevertheless these values are diluted due to the presence of HSF as it does not take part in both the cold crystallization and melting. For this reason, the

 DOI 10.1002/pc

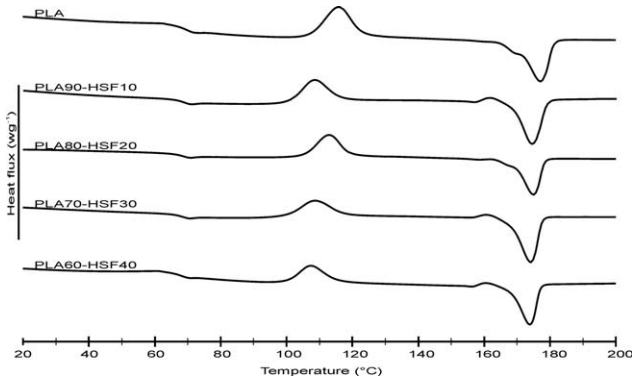

FIG. 4. Comparative plot of DSC curves of unfilled PLA and PLA/HSF composites with different HSF content.

corresponding enthalpies were corrected by considering the real weight of PLA, since PLA is the only component that contributes to cold crystallization and melting. These corrected values appear as ΔH_{cc} corrected and ΔH_m corrected respectively in Table 1. We can see a slight increase in crystallinity as the HSF content increases. This fact indicates a slight nucleating effect of HSF particles that promote crystallization. The chemical nature of the solid lignocellulosic particles favours crystallite formation on PLA/HSF composites. Perinovik et al. have suggested that lignin (which appears in hazelnut shell in a great amount) could act as nucleating agent thus leading to an increase in crystallinity. Though PLA can achieve high crystallinity degree, the final crystallinity is highly affected by the cooling process after injection moulding. For this reason, it is important to remove the previous thermal history. The final crystallinity is a direct consequence of two competing processes; on the one hand, the nucleating effect provided by the lignin and cellulose structures that lead to an increase in crystallinity but on the other hand, the filler particles can act as obstacle for polymer chains to form stable crystals, thus having a negative effect on crystallinity. The overall effect of these two competing process is a slight increase in crystallinity and it is possible to expect that the nucleating effect is slightly higher than that related to the obstacle for crystal formation [4, 8, 11, 30, 42]. With regard to the cold crystallization enthalpy (ΔH_{cc} corrected), we observe a slight increase due to the nucleating phenomena provided by the lignocellulosic filler. The evolution of the melt enthalpy (ΔH_m corrected) is similar and we can observe a slight increase in crystallinity due to the nucleating effect of HSF particles.

Thermal stability of PLA/HSF composites at high temperatures was studied by thermogravymetric analysis (TGA). Figure 5 shows a comparative plot of the TGA and DTG thermograms corresponding to individual PLA and hazelnut shell flour together with the TGA thermograms for all PLA/HSF composites.

The TGA curve of hazelnut shell flour (HSF) is characterized by an initial weight loss of approximately 8 wt% at about 100°C that is related to moisture removal. The highest weight loss is 64 wt%; this wide degradation process starts at about 230°C and it is prolonged up to 500°C. This degradation stage corresponds to the degradation of several components of the lignocellulosic filler. The first components to degrade are hemicellulose (firstly) followed by cellulose and finally lignin degrades at higher temperatures in a wide temperature range. Perinovic et al. determined that polysaccharides such as cellulose and hemicellulose tend to degrade at temperatures in the 220–290°C range while lignin is characterized by a lower degradation rate than cellulose and hemicellulose and consequently, lignin is more heat resistant at high temperatures. It is important to remark that degradation of hemicellulose, cellulose, and lining overlaps but their contribution to the weight loss is different depending on the temperature range. The initial weight loss in the 200–220°C range is mainly attributed to hemicellulose degradation as its degradation rate is higher to that of cellulose and lignin. At higher temperatures, cellulose degradation continues with slower degradation rate than hemicellulose but lignin degradation is still lower as it degrades very slowly [43]. That is why the last degradation section offers a soft slope up to 500°C which corresponds to the slow and progressive degradation of lignin. Finally, the full degradation occurs at about 500°C leading to a carbon char residue that represents almost 28 wt% (mainly ashes from lignin) [4, 14, 23, 43–46].

The TGA curve of unfilled PLA shows an initial section without significant weight loss up to 345°C. Over this temperature, thermal degradation starts. PLA degrades in a quick one-step process in which almost all the weight is lost at temperatures of 368°C. As some authors suggest, the main products from PLA degradation are lactic acid

TABLE 1. Thermal properties of PLA/HSF composites with different HSF content, obtained by differential scanning calorimetry (DSC).

HSF Content (wt%)	T_g (°C)	T_{cc} (°C)	ΔH_{cc} (J g^{-1})	ΔH_{cc} corrected *a* (J g^{-1})	T_m (°C)	ΔH_m (J g^{-1})	ΔH_m corrected*a* (J g^{-1})	X_c (%)
0	66.4 ± 0.2	111.5 ± 0.5	23.6 ± 0.2	23.6	170.8 ± 0.4	−33.8 ± 0.1	−33.8	11
10	66.8 ± 0.4	104.2 ± 0.4	22.2 ± 0.2	24.7	170.8 ± 0.4	−34.1 ± 0.1	−37.9	14
20	66.5 ± 0.4	104.80 ± 0.5	20.9 ± 0.1	26.2	169.9 ± 0.6	−32.4 ± 0.2	−40.5	15
30	66.4 ± 0.3	104.4 ± 0.6	19.0 ± 0.2	27.2	169.5 ± 0.5	−31.1 ± 0.2	−44.5	18
40	66.7 ± 0.5	103.0 ± 0.4	18.0 ± 0.1	30.0	169.1 ± 0.5	−28.0 ± 0.1	−46.7	18

ΔH_{cc} corrected and ΔH_m corrected, correspond to normalized crystallization and melt enthalpies by considering the real weight% PLA on PLA/HSF composites.

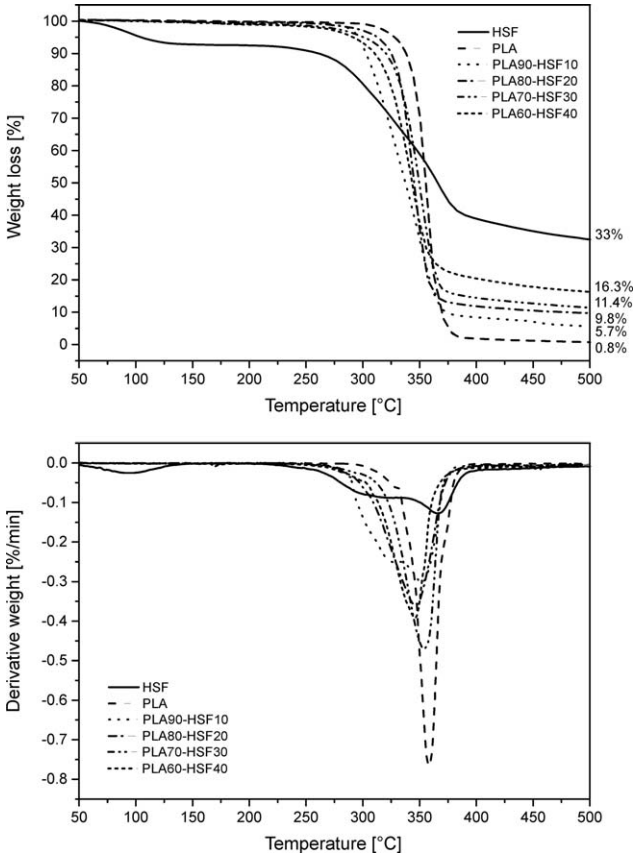

FIG. 5. TGA and DTG curves corresponding to unfilled PLA, hazelnut shell flour (HSF) and PLA/HSF composites with different HSF content.

oligomers, acetaldehydes, carbon dioxide, carbon monoxide, and ketones [4].

TGA curves of PLA/HSF composites show a slight decrease in the onset degradation temperature, changing from 345°C for unfilled PLA up to values in the 306–331°C for all PLA/HSF composites. The initial degradation stage of PLA/HSF composites is related to the HSF degradation. As it has been indicated previously, there is a lack of interaction (or very poor) between HSF particles and the surrounding PLA matrix so that degradation initially proceeds with the lowest thermal stable component (hemicellulose contained in HSF) followed by the more thermally stable components (PLA and lignin from HSF). The residual carbon char is directly related to the HSF content, as PLA does not generates significant amounts of carbon char after full degradation. The degradation process finishes at temperatures of 361–368°C and the weight loss percentage decreases as the HSF increases: 95, 90.6, 90.4, and 85.5 wt% for PLA/HSF composites containing 10, 20, 30, and 40 wt% HSF. In general terms, as hazelnut shell powder is less thermally stable tan PLA, addition of HSF leads to a slight decrease in the thermal stability of PLA which is not a drawback for industrial uses as this decrease is detectable at high temperatures [4, 13, 15, 24, 47].

Table 2 shows some physical properties and parameters representative for the thermomechanical stability of PLA/HSF composites together with the density. As one can see, the density increases slightly as the HSF increases, i.e. for PLA/HSF composites containing 40 wt% HSF density is close to 6% more than unfilled PLA, so that, in general terms, PLA/HSF composites are lightweight materials. With regard to the Vicat softening temperature (VST), it is detectable a remarkable increase in VST values as the HSF content increases. The VST value of unfilled PLA is around 52.8°C and this value increases up to 64.4°C for PLA/HSF composites containing 40 wt% HSF. The evolution of the heat deflection temperature (HDT) is similar but the increase is slightly lower. The increase in the thermomechanical stability is related to two main phenomena: on the one hand, the increase in crystallinity due to the slight nucleating effect provided by the lignocellulosic HSF particles. On the other hand, HSF particles themselves lead to an increase in thermal stability, as they are rigid particles dispersed in a plastic matrix with a positive effect on overall composite stiffness [6, 24]. It is also worth to note that VST and HDT values are directly related to density so that, as density increases (due to crystallinity and packed HSF particles), thermomechanical stability increases.

Figure 6 shows the plot evolution of the coefficient of linear thermal expansion (CLTE) (below and over the glass transition temperature, T_g) of PLA/HSF composites as a function of the HSF content. Below the glass transition temperature T_g, the linear expansion is lower than over the glass transition temperature due to polymer chain mobility. Below the glass transition temperature, polymer chain mobility is highly restricted and this leads lo low linear expansion values. With regard to the evolution of the CLTE below T_g, a decrease in CLTE values as the HSF content increases can be observed thus indicating higher dimensional stability. Unfilled PLA is characterized by a CLTE of 78.41 μm $m^{-1}°C^{-1}$ which is progressively reduced to values of 64.34 μm $m^{-1}°C^{-1}$, 61.07 μm $m^{-1}°C^{-1}$, and 54.91 μm m^{-1} for PLA/HSF composites containing 20, 30, and 40 wt% HSF respectively. With regard to the evolution of CLTE values over the glass transition temperature, it is possible to observe similar tendency but with higher values due to higher chain mobility. The CLTE of unfilled PLA over the T_g is 171.4 μm $m^{-1}°C^{-1}$ and this is reduced up to 167.8 μm $m^{-1}°C^{-1}$ with the sole addition of 10 wt% HSF. All the CLTE values for PLA/HSF composites are lower than the value corresponding to unfilled PLA. Similar findings have been reported for PLA-based

TABLE 2. Vicat softening temperature (VST), heat deflection temperature (HDT), and density of unfilled PLA and PLA/HSF composites with different HSF content.

HSF content (wt%)	VST (°C)	HDT (°C)	Density (g cm^{-3})
0	52.8 ± 0.7	47.6 ± 2.2	1.18 ± 0.04
10	54.1 ± 1.8	53.1 ± 3.2	1.19 ± 0.03
20	54.5 ± 2.1	53.1 ± 4.1	1.20 ± 0.03
30	58.4 ± 0.8	54.6 ± 2.5	1.23 ± 0.05
40	64.4 ± 2.5	54.5 ± 1.3	1.26 ± 0.04

DOI 10.1002/pc

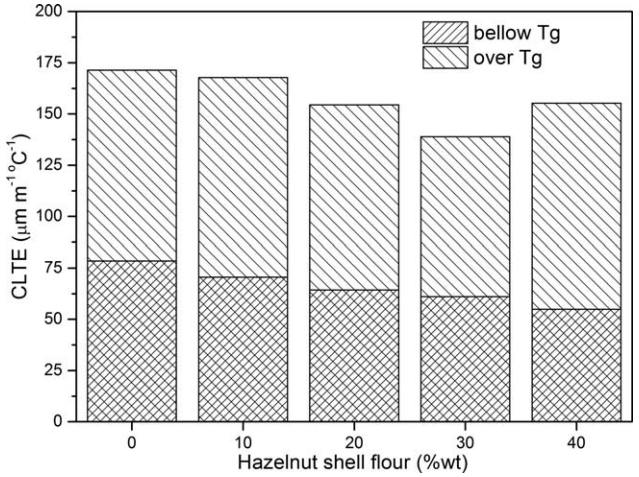

FIG. 6. Bar plot of the evolution of the coefficient of linear thermal expansion (CLTE) for PLA/HSF composites with different HSF content.

composites regarding mechanical and thermomechanical properties [48, 49].

Dynamic mechanical thermal analysis (DMTA) allows evaluating PLA/HSF composites in dynamic load conditions as a function of temperature. Figure 7 shows the comparison of the storage modulus (G') in terms of temperature for PLA/HSF composites. It is clearly observable the temperature dependence of the storage modulus. Below the glass transition temperature, T_g, PLA/HSF composites behave as elastic materials with high G' values. In the temperature range comprised between 30 and 60°C, the storage modulus, G' curve is moved towards higher G' values as the HSF content increases thus indicating that addition of HSF filler to PLA leads to stiffer materials. Table 3 shows a summary of the storage modulus, G' at four different temperatures. At 30°C, G' of unfilled PLA is 1380 MPa and this value is increased up to 2392 MPa for PLA/HSF composite containing 30 wt% HSF which represents almost a 74% increase.

At about 60°C, we observe a dramatic decrease in the storage modulus due to the glass transition temperature

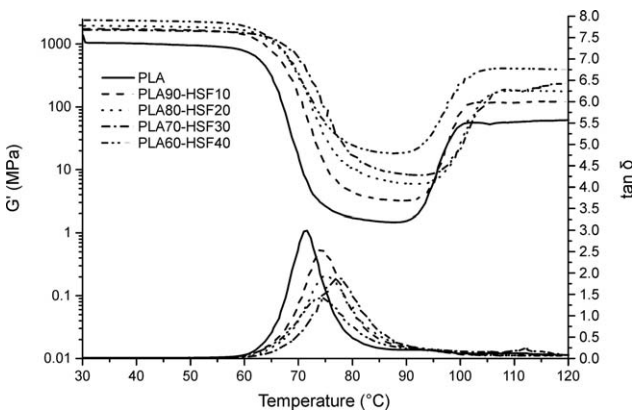

FIG. 7. Comparative plot of the DMTA curves (storage modulus, G' and damping factor tan δ) for PLA/HSF composites with different HSF content.

TABLE 3. Effect of the hazelnut shell flour (HSF) content on the storage modulus (G') of PLA/HSF composites at four different temperatures.

HSF content (wt%)	Storage modulus, G' (MPa)			
	At 30°C	At 50°C	At 90°C	At 120°C
0	1380 ± 4	954 ± 6	1.54 ± 0.21	61.74 ± 0.51
10	1737 ± 7	1661 ± 8	3.22 ± 0.14	119.83 ± 0.42
20	1935 ± 8	1877 ± 8	5.99 ± 0.09	177.25 ± 0.98
30	1677 ± 5	1615 ± 4	8.34 ± 0.08	233.82 ± 0.62
40	2392 ± 2	2272 ± 8	18.99 ± 0.32	393.10 ± 1.01

range (T_g). In Table 3, it is possible to detect that G' values at 90°C are similar to rubbers. Despite this, the same tendency described for G' below T_g is observed. Lignocellulosic particles restrict polymer chain mobility and this gives stiffer materials. Over 90°C an increase in storage modulus can be observed; this phenomenon is related to the cold crystallization of PLA. Polymer chains rearrange to a more packed structure thus leading to an increase in mechanical response. The cold crystallization increases density due to a more packaged structure and subsequently, the storage modulus is also increased [12]. As one can see, the cold crystallization temperature decreases due to the nucleating effect that lignocellulosic particles can provide. This decrease is in total agreement with previous DSC results. As previously described, two overlapping phenomena can be produced by the lignocellulosic filler: on the one hand, a nucleating effect can lead to increased crystallinity but on the other hand, dispersed lignocellulosic particles can obstacle chain packing with a negative effect on crystallinity. Both processes occur simultaneously but the nucleating effect is clearly evident through the observation of the cold crystallization process in both DMTA and DSC analysis. Table 3 shows that the storage modulus increases up to values in the 100–400 MPa range due to the cold crystallization. As expected, the crystallization is more intense for PLA/HSF composites with higher HSF content which leads to higher storage modulus after cold crystallization, i.e., G' at 120°C for PLA/HSF composite with 40 wt% HSF is six times higher than unfilled PLA at the same temperature. Presence of lignocellulosic particles contributes to stiffer materials by promoting crystallization and by restricting polymer chain mobility [10, 42].

Figure 7 also shows the comparison of the damping factor (tan δ) for PLA/HSF composites with varying HSF load. The highest peak corresponds to unfilled PLA. As the HSF content increases, a decrease in the peak height related to the dilution effect provided by hazelnut shell filler can be observed. In addition, it is possible to detect a displacement of the peak towards slightly higher temperatures, which is related to some restrictions for polymer chain motion (slight increase in T_g) in the surrounding area around the dispersed HSF particles. As previously indicated, the lignocellulosic filler can obstacle polymer chains thus making difficult the chains to pack. It is also possible to observe a small hump

TABLE 4. Mechanical properties of PLA/HSF composites with different HSF content.

HSF content (wt%)	Flexural modulus (GPa)	Flexural strength (MPa)	Impact absorbed energy (KJ m^{-2})	Shore D hardness (HS_D)
0	3.24 ± 0.05	108.5 ± 2.2	16.5 ± 1.2	70.2 ± 0.5
10	3.74 ± 0.04	101.1 ± 3.8	14.6 ± 1.8	74.0 ± 1.2
20	3.93 ± 0.09	83.7 ± 1.8	12.4 ± 2.6	75.6 ± 0.5
30	4.54 ± 0.09	75.8 ± 1.7	10.0 ± 1.5	76.6 ± 0.5
40	4.73 ± 0.04	67.6 ± 2.9	8.7 ± 1.3	78.4 ± 0.9

in the temperature range comprised between 90°C and 100°C which is related to the cold crystallization process as described previously [7, 10, 12].

Mechanical Properties of PLA/HSF Composites

Table 4 summarizes the main parameters from mechanical tests of PLA/HSF composites. All PLA/HSF composites show a higher flexural modulus as expected. Composites containing 40 wt% HSF offer a flexural modulus of 4.73 GPa which is remarkably higher if compared to unfilled PLA with a flexural modulus of 3.24 GPa. In general, addition of lignocellulosic particles leads to stiffer materials in terms of modulus as previously observed by DMTA. Nevertheless, the flexural strength decreases as the hazelnut shell content increases. The maximum flexural strength is achieved for unfilled PLA with 108 MPa and this reference value is reduced up to 67 MPa for PLA/HSF composites with 40 wt% HSF. This remarkable decrease is related to poor particle–polymer interactions, which lead to embrittlement. Load transfer from particles to the matrix is not good due to the lack of interaction between the dispersed HSF particles and the surrounding PLA matrix so that, dispersed particles act as stress concentrators. As the hazelnut shell content increases, the matrix–particle continuity is lost in a great extent and this leads to early fracture [2, 6, 7, 9, 11, 12, 17, 27, 44].

Table 4 also shows the values of impact absorbed energy for PLA and PLA/HSF composites. The impact resistance of unfilled PLA is 16.5 kJ m^{-2} and this is remarkably reduced up to the half for composites with 40 wt% HSF (8.7 kJ m^{-2}). This important decrease is due to poor particle–polymer interactions as described before. The lack of strong interactions between the dispersed HSF particles and the surrounding PLA matrix promotes microcrack formation and subsequent growing due to stress concentration during impact conditions.

On the other hand, as the hazelnut shell content increases, shore hardness increases. Table 4 shows that the hardness of PLA/HSF with 10 wt% HSF is close to 71 HS_D and this is increased up to 78 HS_D for composites containing 40 wt% HSF. This increase is in total agreement with previous results; the addition of a more stiff lignocellulosic filler together with the crystallinity increase provided by the nucleating phenomena, leads to increased hardness values [12, 14, 17, 23].

CONCLUSIONS

The results obtained in this study indicate that hazelnut shell flour, a byproduct of the food industry, can optimally be used as reinforcing filler in fully biodegradable composites with poly(lactic acid)–PLA matrix. These composites offer high environmental efficiency and they can positively contribute to sustainable development. Characterization of PLA/HSF composites shows that addition of HSF in particle form leads to stiffer materials (as much stiffer as the HSF content increases). Lignocellulosic hazelnut shell particles provide a slight nucleating effect on poly(lactic acid) chains thus leading to an increase in crystallinity which has a positive effect on dimensional stability of PLA/HSF composites together with highly dispersed HSF that act as interlock points. The storage modulus, G', increases in a remarkable way with the hazelnut shell content. This situation is even more pronounced in the temperature range comprised between 90°C and 100°C due to the crystallization promoted by dispersed HSF particles. The flexural modulus increases in a remarkable way but the impact absorbed energy decreases up to values around the half value of unfilled PLA. SEM study reveals the lack of strong HSF particle–PLA matrix interactions and this is responsible for stress concentration phenomena that promotes early fracture.

Globally this study defines the potential of PLA/HSF composites for uses that require high stiffness together with high dimensional stability. The thermoplastic nature of this materials allows easy processing by conventional extrusion + injection moulding processes with high filler content up to 40 wt% and attractive wood-like surface finishing. PLA-based green composites with a hazelnut shell flour content in the 30–40 wt% are the most attracting formulations from an industrial point of view as they offer balanced mechanical properties, full biodegradability and a remarkable decrease in material cost. These formulations could find applications as wood plastic composites (WPCs) in the building industry (fencing, decking, flooring, etc.), automotive interior parts and furniture.

REFERENCES

1. L. Averous, *J. Macromol. Sci. Polym. Rev.*, **C44**, 231 (2004).
2. T. Mukherjee and N. Kao, *J. Polym. Environ.*, **19**, 714 (2011).
3. O. Martin and L. Averous, *Polymer*, **42**, 6209 (2001).

 DOI 10.1002/pc

4. S. Perinovic, B. Andricic, and M. Erceg, *Thermochim. Acta*, **510**, 97 (2010).
5. K. Madhavan Nampoothiri, N.R. Nair, and R.P. John, *Bioresour. Technol.*, **101**, 8493 (2010).
6. K.W. Kim, B.H. Lee, H.J. Kim, K. Sriroth, and J.R. Dorgan, *J. Therm. Anal. Calorim.*, **108**, 1131 (2012).
7. S. Li, C. Wang, X. Zhuang, Y. Hu, and F. Chu, *J. Polym. Environ.*, **19**, 301 (2011).
8. Y. Li, K. Venkateshan, and X.S. Sun, *Polym. Int.*, **59**, 1099 (2010).
9. R. Liu, J. Cao, S. Luo, and X. Wang, *J. Appl. Polym. Sci.*, **127**, 2566 (2013).
10. A.P. Mathew, K. Oksman, and M. Sain, *J. Appl. Polym. Sci.*, **97**, 2014 (2005).
11. S. Pilla, S. Gong, E. O'Neill, R.M. Rowell, and A.M. Krzysik, *Polym. Eng. Sci.*, **48**, 578 (2008).
12. B.L. Shah, S.E. Selke, M.B. Walters, and P.A. Heiden, *Polym. Compos.*, **29**, 655 (2008).
13. Y.F. Shih, C.C. Huang, and P.W. Chen, *Mater. Sci. Eng. A: Struct. Mater. Properties Microstruct. Process.*, **527**, 1516 (2010).
14. A.A. Yussuf, I. Massoumi, and A. Hassan, *J. Polym. Environ.*, **18**, 422 (2010).
15. Y.F. Shih and C.C. Huang, *J. Polym. Res.*, **18**, 2335 (2011).
16. H.M. Akil, M.F. Omar, A.A.M. Mazuki, S. Safiee, Z.A.M. Ishak, and A. Abu Bakar, *Mater. Des.*, **32**, 4107 (2011).
17. E. Petinakis, L. Yu, G. Edward, K. Dean, H. Liu, and A.D. Scully, *J. Polym. Environ.*, **17**, 83 (2009).
18. B. Ferrero, V. Fombuena, O. Fenollar, T. Boronat, and R. Balart, *Polym. Compos.*, **36**, 1378 (2015).
19. M.A. Moreira de Araujo, A.R. de Sena Neto, E. Hage, Jr., L.H. Capparelli Mattoso, and J.M. Marconcini, *Polym. Compos.*, **36**, 1520 (2015).
20. E. Olewnik and J. Richert, *Polym. Compos.*, **36**, 17 (2015).
21. C.Y. Tsou, C.L. Wu, C.H. Tsou, S.H. Chiu, M.C. Suen, and W.S. Hung, *Polym. Sci. Ser. B*, **57**, 473 (2015).
22. T. Qiang, D. Yu, A. Zhang, H. Gao, Z. Li, Z. Liu, W. Chen, and Z. Han, *J. Cleaner Prod.*, **66**, 139 (2014).
23. K. Salasinska and J. Ryszkowska, *Compos. Interfaces*, **19**, 321 (2012).
24. S. Singh and A.K. Mohanty, *Compos. Sci. Technol.*, **67**, 1753 (2007).
25. A.K. Mohanty, M. Misra, and L.T. Drzal, *J. Polym. Environ.*, **10**, 19 (2002).
26. I. Naghmouchi, F.X. Espinach, P. Mutje, and S. Boufi, *Mater. Des.*, **65**, 454 (2015).
27. N. Petchwattana and S. Covavisaruch, *J. Bionic Eng.*, **11**, 630 (2014).
28. J. Summerscales, N. Dissanayake, A. Virk, and W. Hall, *Appl. Sci. Manufact.*, **41**, 1336 (2010).
29. G. Bogoeva-Gaceva, M. Avella, M. Malinconico, A. Buzarovska, A. Grozdanov, G. Gentile, and M.E. Errico, *Polym. Compos.*, **28**, 98 (2007).
30. E. Parparita, R.N. Darie, C.-M. Popescu, M.A. Uddin, and C. Vasile, *Mater. Des.*, **56**, 763 (2014).
31. M.U. Wahit, N.I. Akos, and W.A. Laftah, *Polym. Compos.*, **33**, 1045 (2012).
32. K. Piekarska, E. Piorkowska, N. Krasnikova, and P. Kulpinski, *Polym. Compos.*, **35**, 747 (2014).
33. A. Nourbakhsh and A. Ashori, *Bioresour. Technol.*, **101**, 2525 (2010).
34. B. Ferrero, T. Boronat, R. Moriana, O. Fenollar, and R. Balart, *Polym. Compos.*, **34**, 1663 (2013).
35. Y. Copur, C. Guler, M. Akgul, and C. Tascioglu, *Build. Environ.*, **42**, 2568 (2007).
36. C. Stevigny, L. Rolle, N. Valentini, and G. Zeppal, *J. Sci. Food Agric.*, **87**, 2817 (2007).
37. Y. Xu, E.N. Sismour, J. Parry, M.A. Hanna, and H. Li, *Int. J. Food Sci. Technol.*, **47**, 940 (2012).
38. E.W. Fischer, H.J. Sterzel, and G. Wegner, *Kolloid-Zeitschrift and Zeitschrift Fur Polymere*, **251**, 980 (1973).
39. T.Y. Ke and X.Z. Sun, *J. Appl. Polym. Sci.*, **81**, 3069 (2001).
40. A. Csikos, G. Faludi, A. Domjan, K. Renner, J. Moczo, and B. Pukanszky, *Eur. Polym. J.*, **68**, 592 (2015).
41. S. Lv, H. Tan, J. Gu, and Y. Zhang, *Bioresources*, **10**, 5426 (2015).
42. A.P. Mathew, K. Oksman, and M. Sain, *J. Appl. Polym. Sci.*, **101**, 300 (2006).
43. V. Tserki, P. Matzinos, S. Kokkou, and C. Panayiotou, *Compos. A: Appl. Sci. Manufact.*, **36**, 965 (2005).
44. X. Li, B. Lei, Z. Lin, L. Huang, S. Tan, and X. Cai, *Mater. Des.*, **53**, 419 (2014).
45. V. Matejka, Z. Fu, J. Kukutschova, S. Qi, S. Jiang, X. Zhang, R. Yun, M. Vaculik, M. Heliova, and Y. Lu, *Mater. Des.*, **51**, 847 (2013).
46. N.F.M. Rawi, K. Jayaraman, and D. Bhattacharyya, *Polym. Compos.*, **35**, 1888 (2014).
47. N. Dehbari, N. Moazeni, and W.A. Rahman, *Polym. Compos.*, **35**, 1220 (2014).
48. P. Georgiopoulos, E. Kontou, and M. Niaounakis, *Polym. Compos.*, **35**, 1140 (2014).
49. R. Liu, J. Cao, Y. Peng, and Y. Chen, *Polym. Compos.*, **36**, 731 (2015).